Influence of thermal stratification on the structure and evolution of the Martian core.

Sam Greenwood[1], Christopher J. Davies[1], and Anne Pommier[2]

[1]University of Leeds
[2]UC San Diego

November 26, 2022

Abstract

The apparent end of the internally generated Martian magnetic field at 3.6-4.1 Ga has been linked to insufficient core cooling. While the dynamo cessation time is a key event in the Martian history, a large range of solutions exist to satisfy this observation, limiting the insight it provides on the Martian interior. We produce a suite of models improving our understanding of the evolution of Mars in three keys areas. Firstly, we account for thermal stratification in the core, producing improved estimates on the core thermal structure. Secondly, we match estimates for the present-day areotherm. Finally, we consider recent experimental data for the core thermal conductivity, k_c, much lower than previously thought for Mars. In order to yield a consistent dynamo cessation time we require k_c<18 $Wm^{-1}K^{-1}$. Furthermore, the majority of our models indicate the core is fully conductive at present and too hot to form any solid.

Influence of thermal stratification on the structure and evolution of the Martian core.

Sam Greenwood[1], Christopher J. Davies[1], Anne Pommier[2,3]

[1]School of Earth and Environment, University of Leeds, Leeds, UK
[2]Scripps Institution of Oceanography, University of California San Diego, La Jolla, CA, USA
[3]Earth and Planets Laboratory, Carnegie Institution for Science, Washington, DC, USA

Key Points:

- Present day core temperature profile is conductive rather than the frequently assumed isentropic state.
- End of internal magnetic field on Mars places limits on the thermal conductivity of the core.
- Estimates of the mantle temperature are a useful additional constraint, limiting the range of mantle viscosities in successful solutions.

Corresponding author: Sam Greenwood, `s.greenwood@leeds.ac.uk`

Abstract

The apparent end of the internally generated Martian magnetic field at 3.6-4.1 Ga has been linked to insufficient core cooling. While the dynamo cessation time is a key event in the Martian history, a large range of solutions exist to satisfy this observation, limiting the insight it provides on the Martian interior. We produce a suite of models improving our understanding of the evolution of Mars in three keys areas. Firstly, we account for thermal stratification in the core, producing improved estimates on the core thermal structure. Secondly, we match estimates for the present-day areotherm. Finally, we consider recent experimental data for the core thermal conductivity, k_{c}, much lower than previously thought for Mars. In order to yield a consistent dynamo cessation time we require $k_{\mathrm{c}} \geq 18$ W m^{-1}K^{-1}. Furthermore, the majority of our models indicate the core is fully conductive at present and too hot to form any solid.

1 Introduction

Unlike Earth, Mars does not possess an internally generated global magnetic field. However, analysis of vector magnetic measurements from the MGS and MAVEN satellites reveals remnant magnetisation characteristic of magnetisation formed in the presence of a much stronger magnetic field than exists today (Acuna et al., 1998; Langlais et al., 2019). The remnant magnetisation appears in crustal rocks older than an estimated 3.6-4.1 Ga (Acuna et al., 1998; Langlais et al., 2012; Milbury et al., 2012; Mittelholz et al., 2020), leading to the common theory that an early dynamo on Mars generated a large scale field prior to these age estimates (Stevenson, 2001). The dynamo process is produced by fluid convection of iron-alloy in the core, where thermal buoyancy is created by the mantle conducting heat away from the core and potentially chemical buoyancy provided by freezing liquid (Nimmo & Stevenson, 2000; Stevenson, 2001; Williams & Nimmo, 2004; Davies & Pommier, 2018). The magnetic history of Mars is therefore intimately linked to the evolution of the planet as it cools over geological time.

Analysing the thermal and magnetic evolution of the Martian core requires two dimensional (radius and time) parameterised thermal history models to simulate the long timescales (Myrs-Gyrs) associated with the slow loss of heat from the planet. A key quantity is the heat extracted from the core by the mantle at the Core-Mantle Boundary (CMB), Q_c, relative to the heat flow down an isentropic temperature gradient resulting from convection, Q_a. In the absence of freezing, a dynamo fails very close to the transition from a super-isentropic heat flow ($Q_\mathrm{c} > Q_\mathrm{a}$) to a sub-isentropic heat flow ($Q_\mathrm{c} < Q_\mathrm{a}$) (Nimmo, 2015). As such, the thermal evolution of both the core and mantle must be solved to estimate Q_c as a function of time, which in turn allows analysis of the magnetic history of Mars.

A variety of solutions for the evolution of Mars have been proposed, exhibiting a range of physical processes. Nimmo and Stevenson (2000) suggested that a brief period of plate tectonics before a transition to stagnant lid tectonics was required to cool the planet to power a dynamo prior to $\sim$4 Ga. Due to a lack of evidence for plate tectonics on Mars, Williams and Nimmo (2004) instead showed that an initially super-heated core relative to the mantle provides the required short period of rapid cooling to power the dynamo. Growth of a large inner core would have likely restarted the dynamo (Williams & Nimmo, 2004) but recent growth of a small inner core might not yet be able to provide enough compositional buoyancy and could restart the dynamo in the future (Hemingway & Driscoll, 2021). Depending upon the relative slopes of the core temperature and its melting temperature, the core may instead start to freeze from the top-down rather than bottom-up (Stewart et al., 2007). In this freezing regime, iron freezes as a snow at the top of the core, sinking deeper into the core and remelting, releasing additional power for a dynamo. The amount of power is relatively small compared to a growing inner core and so a snow zone could be present today without restarting the dynamo (Davies & Pommier, 2018). All previous studies generally agree that the Martian core is required to have undergone a short period of rapid cooling, powering the dynamo, before the cooling rate of the planet becomes too low to sustain the dynamo after $\sim 3.6 - 4.1$ Ga.

There are three main issues that may alter our view of the Martian evolution. Firstly, Q_a is proportional to the thermal conductivity of the core, k_c. The magnetic history of Mars is therefore very sensitive to k_c, given the above condition on Q_c relative to Q_a for dynamo action. Recent experimental studies on a variety of iron-alloys at conditions appropriate for Mars have yielded values for k_c from as low as 5 W m^{-1}K^{-1} to around 30 W m^{-1}K^{-1}, depending on the precise composition (Pommier, 2018; Pommier et al., 2020). These conductivities are lower than those used in previous models of Mars, which have typically used 40 W m^{-1}K^{-1} (Nimmo & Stevenson, 2000; Williams & Nimmo, 2004; Davies & Pommier, 2018), whereas Hemingway and Driscoll (2021) consider a range of $k_\mathrm{c} = 30 - 120$ W m^{-1} K^{-1}. A significantly lower k_c alters the ability for the core generate a magnetic field (Pommier et al., 2020) and therefore can change our understanding of the evolution of the planet.

Secondly, all previous models predict that the Martian core was heavily sub-isentropic ($Q_\mathrm{c} < Q_\mathrm{a}$) for a significant proportion of its history, including at present. When sub-isentropic, the thermal state of the core deviates away from a convective state towards a conductive one, resulting in a stable, thermally stratified layer that grows from the top of the core downwards (Labrosse et al., 1997; Nimmo, 2015; Greenwood et al., 2021), assuming chemical convection is not present or insufficient to mix the layer away. Previous models for Mars have assumed that even when $Q_\mathrm{c} < Q_\mathrm{a}$, the core remains convecting, limiting predictions for the present day temperature of the core. The change in core temperature from thermal stratification also alters the timing for freezing of solid as well as influencing the evolution of Q_c. By accounting for thermal stratification we can more precisely estimate the present day core temperature, complimenting other modelling techniques (e.g. Rivoldini et al., 2011; Plesa et al., 2018; Khan et al., 2018) and observations from missions such as InSight to understand the interior structure of Mars that are not as sensitive to the core temperature. Thirdly, improved geophysical inversions for the present day areotherm (Khan et al., 2018) offer an additional constraint upon evolution models not previously utilised. In this paper we produce a suite of thermal history models addressing each of these 3 areas.

2 Methods

We solve for the thermal evolution of Mars by coupling parameterised convection models for the core and mantle. The core is assumed to be well mixed with an adiabatic temperature profile. When Q_c becomes smaller than the heat conducted along the adiabatic profile, a stratified layer grows beneath the CMB with a conductive temperature profile. We used a common approach for the Martian mantle with an isothermal convecting interior bounded by thermal boundary layers above the CMB and beneath a stagnant lid (Williams & Nimmo, 2004; Thiriet et al., 2019). Linear temperature profiles are assumed in the thermal boundary layers and across the stagnant lid.

For the core, we use the model of Greenwood et al. (2021), which accounts for a stable layer in a standard energy balance to evolve the core temperature. An entropy balance is then used to estimate the ohmic dissipation produced by magnetic field generation, E_J (Gubbins et al., 2003; Williams & Nimmo, 2004; Greenwood et al., 2021):

$$E_\mathrm{J} = E_\mathrm{s} - E_\mathrm{k}, \tag{1}$$

where E_k, E_s, and E_J refer to the changes in entropy arising from thermal conduction, secular cooling, and ohmic dissipation within the core. Since $E_\mathrm{k} \propto k_\mathrm{c}$, a smaller k_c gives a smaller E_k and hence a larger E_J. Dynamo action is inferred when E_J becomes larger than 1 MW K^{-1} which occurs close to, but not precisely, the condition $Q_\mathrm{c} > Q_\mathrm{a}$. Whilst our model for the core can account for solidification of either a solid core or iron snow (Davies & Pommier, 2018; Greenwood et al., 2021), we do not find scenarios where any core fluid freezes and so do not include their associated terms in Equations 1. See supplementary text S1 for further details on the entropy budget.

The mantle is modelled using the parameterisation of stagnant lid convection of Thiriet et al. (2019). Temperature dependent mantle viscosity in the upper/lower thermal boundary layers are evaluated at the average temperatures within the relevant boundary layer given an Arrhenius equation, scaled by a reference viscosity η_0 at a reference temperature of 1600 K

$$\eta(T) = \eta_0 \exp\left(\frac{A}{R}\left[\frac{1}{T} - \frac{1}{1600}\right]\right), \tag{2}$$

where A is the activation energy, taken to be 300 kJmol^{-1} assuming diffusion creep (Karato & Wu, 1993), and R is the gas constant. The temperature of the upper mantle beneath the stagnant lid, $T_{\mathrm{m,u}}$, is scaled from the isothermal convecting mantle temperature as $T_{\mathrm{m,u}} = T_{\mathrm{m}} - aRT_{\mathrm{m}}^2/A$, where a is a fixed constant. We take $a = 2.54$ with a corresponding β factor of 0.335 used for scaling the boundary layer thickness which are the best fitting values of Thiriet et al. (2019). In general, a larger η_0 or lower T_{m} thickens the thermal boundary layers, reducing Q_{c} for a given temperature difference between mantle and core. The thickness of the stagnant lid was fixed to 300 km rather than being time dependent since we find this has no significant effect upon the evolution of Mars (Supplementary figure S1). Models are iterated from 4.5 Ga until present day from their initial conditions.

Roughly 8 wt% nickel is expected in the Martian core (Wänke & Dreibus, 1994), along with 10-20 wt% sulphur (Rivoldini et al., 2011; Khan et al., 2018) and as such we assumed an Fe-Ni-S core. We used the melting data of Gilfoy and Li (2020), who observed the melting point of Fe-Ni-S at $\sim$ 1500 K with 10 wt% S at CMB pressure. This low melting temperature suggests that the entire core is liquid at present and, as mentioned above, we find no scenarios where any solid is formed. One consequence of no solid in our calculations is that the composition of the liquid core is constant in time and the amount of Ni/S only influence the material properties of the core.

A number of parameters for Mars are known well enough to be taken as constant in our study, listed in table S1. For example, the radius and density of the core have been constrained to 1730-1840 km and 6100-6500 kg m^{-3} (Khan et al., 2018). Changing these parameters within their uncertainties does not appreciably alter the evolution of the planet relative to some key unknowns, in particular the initial conditions. To address parameters with large uncertainties, we perform Monte-Carlo simulations in order to search the parameter space. We vary the initial temperature of the mantle and core, described by $T_{\mathrm{m,0}}$ and the initial super-heat of the core relative to the mantle, $\Delta T = T_{\mathrm{c}} - T_{\mathrm{m,0}}$, where T_{c} is the CMB temperature. There is little constraint upon the initial core and mantle temperature and due to the thermostat effect, there is limited sensitivity of the initial conditions on the present day state (Plesa et al., 2015). The initial conditions do impact the early evolution of the planet and so are important when considering the longevity of the dynamo. We therefore consider a wide range for $T_{\mathrm{m,0}}$ and ΔT. We also vary the reference viscosity of the mantle, η_0, which has a wide range of proposed values and significantly influences the cooling of the planet. Finally, we are interested in a range of core thermal conductivities, k_{c}. We choose the range 5-40 W m^{-1}K^{-1} based on the results of (Pommier, 2018; Pommier et al., 2020; Pommier, 2020) representing a range of core compositions. As mentioned, our core composition is constant in time in our models since we have no formation of solid to unevenly partition alloying light elements. The effect of composition is therefore limited to the impact upon the material properties of the core, of which k_{c} is most significantly influenced. The density and specific heat capacity are also composition dependent, however, they have an insignificant impact upon the thermal evolution relative to k_{c}.

We ran a large number of models (n=100,000), drawing a random value from a uniform prior for each of the 4 variables between the ranges given in table 1. All other fixed parameters are listed in table S1.

Successful models satisfy two constraints. Firstly, the dynamo cessation time, denoted t_Φ, must be consistent with the magnetic field history of Mars, where the dynamo shut off between 4.1-3.6 Ga (400-900 Myr after core formation) (Acuna et al., 1998; Langlais et al., 2012; Milbury et al., 2012; Mittelholz et al., 2020). Secondly, we choose models from our ensemble that are consistent with estimates of the present day temperature of Mars, using the recent estimates of the areotherm from Khan et al. (2018) based on inversions from geophysical data. Their model is not particularly sensitive to the CMB temperature since they cannot resolve the temperature change in the lower mantle thermal

Table 1. Variables for the parameter search

Parameter	Symbol	Value	Units	Reference
Core thermal conductivity	k_c	5-40	W $m^{-1}K^{-1}$	Pommier et al. (2020)
Core super heat	ΔT	0-500	K	-
Initial Mantle temperature	$T_{m,0}$	1400-2200	K	-
Reference viscosity	η_0	$10^{18} - 10^{21}$	Pa s	Breuer and Spohn (2006); Fraeman and Korenaga (2010)

boundary layer, and so instead we focus on the temperature at the base of the stagnant lid. We identify models with $T_{m,u} = 1650 - 1750$ K as successful in this regard.

3 Results

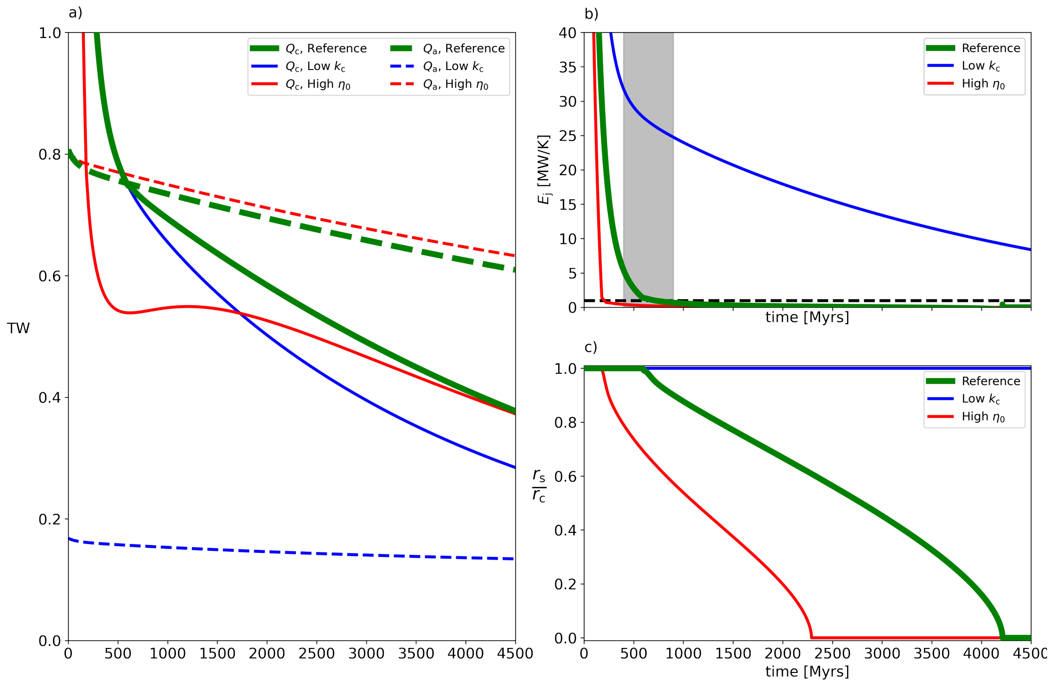

Figure 1. Time series for the 3 example cases described in the text. Panel a) shows the CMB heat flow, Q_c, (solid lines) and the heat flow down the adiabatic temperature gradient at the CMB, Q_a. Panel b) shows the entropy due to ohmic dissipation, E_J. Finally, c) shows the growth of the thermally stratified layer by plotting the radius of the base of the layer, r_s, normalised to the core radius, r_c. The reference case is an example of a successful model, yet the low k_c and high η_0 cases are both unsuccessful.

We first show the time series of three example cases to demonstrate the impact of varying thermal conductivity and mantle viscosity on the evolution of the planet (Fig. 1) as these will be important for interpreting the trends seen in the Monte-Carlo results. The reference case is a successful model taken from the Monte-Carlo simulation (T_m =

2327 K, $\Delta T = 192$ K, $k_c = 24$ W m^{-1}K^{-1}, $\eta_0 = 2.5 \times 10^{20}$ Pa s), whereas the other two cases are unsuccessful. A low conductivity case uses the same input parameters as the reference case, with the exception that k_c is lowered to 5 W m^{-1}K^{-1}, the lowest value we consider. Finally a high viscosity case uses the same input parameters as the reference case except that η_0 is raised to 10^{21} Pa s, the largest value we consider.

In all cases there is an initially super-isentropic heat flow that drops rapidly, before becoming more steady for the majority of time (Fig. 1a). Comparing the reference case to the low conductivity case shows the identical evolution of Q_c until ~ 500 Myr. After this time, the reference case becomes sub-isentropic ($Q_c < Q_a$) and a stable layer begins to grow causing the evolution between them to diverge. The introduction of the stable layer in the reference case relatively elevates the core temperature, leading to a larger temperature difference between the core and mantle, driving a larger heat flow at the CMB. A stable layer never grows in the low conductivity case due to the extremely low values for Q_a. Whilst the stable layer elevates the core temperature, the resulting increase in Q_c increases core cooling to offset this initial increase in temperature. Models that grow a stable layer are generally ~ 30 K hotter at present than if a stable layer were not accounted for. This difference in temperature is small relative to uncertainties in geophysical estimations of the interior temperature but at the low cooling rates of the core still represents ~ 250 Myr worth of core cooling.

Comparing next the high viscosity case to the reference case, as expected, Q_c is decreased since the more viscous mantle produces thicker thermal boundary layers, through which less heat is conducted. Q_c drops off more rapidly, although Q_c is comparable to the reference case at the present day (Fig. 1a). Figure 1c shows the growth of the stable layer through time. The lower heat flows in the high viscosity case result in the stable layer growing sooner and faster than the reference case. The whole core is stratified in both the reference and high viscosity cases by the present day. When the stable layer is thin, the expected growth rate is $\propto \sqrt{\text{time}}$, however, as the heat flow continues to drop and the layer grows there is an acceleration in the growth rate when only a small portion of the core is still convecting ($r_s/r_c < 0.4$). This acceleration is due to the fact that as the convecting region becomes smaller, its mass decreases $\propto r^3$, whereas the heat extracted from it is $\propto r^2$. This results in rapid cooling of the convecting region relative to the stable layer and subsequent rapid movement of r_s.

The effects of η_0 and k_c on E_J can be seen in Figure 1b. The low conductivity case predicts a dynamo operating at all times due to the low entropy associated with thermal conduction, E_k, and is therefore inconsistent with oberservations. The reference and high viscosity case both drop quickly early on, falling below 1 MW K^{-1} (dashed line), our assumed limit for dynamo action, coinciding with the growth of the stable layer. Note that in our entropy budget E_J does not fall below 0, as is physically expected, since accounting for the correct temperature profile when sub-isentropic ensures entropy is balanced (see supplementary text S1 for more details).

The left panel of Figure 2 shows the correlation between the dynamo cessation time, t_Φ, with the present day upper mantle temperature $T_{m,u}$ for the whole ensemble of models. Many models fit either the constraint upon $T_{m,u}$ (n=26,180) or t_Φ (n=9040) but only 2010 models fall within the limits for both. No correlation between $T_{m,u}$ and t_Φ exists as t_Φ is primarily sensitive to heat flows rather than temperatures. The colour scale shows that there is also no correlation between models that fit the dynamo constraint ($t_\Phi = 400-900$ Myr) and the mantle viscosity. There is however a strong correlation between $T_{m,u}$ and η_0 where higher viscosities limit the heat release through the upper mantle thermal boundary layer, insulating the planet and producing a hotter present day mantle by approximately $T_{m,u} \propto \log(\eta_0)$. As such, the present day areotherm offers a complementary constraint to the dynamo cessation time since it limits the reference viscosity in our models to $\eta_0 \sim 10^{20} - 10^{21}$ Pa s.

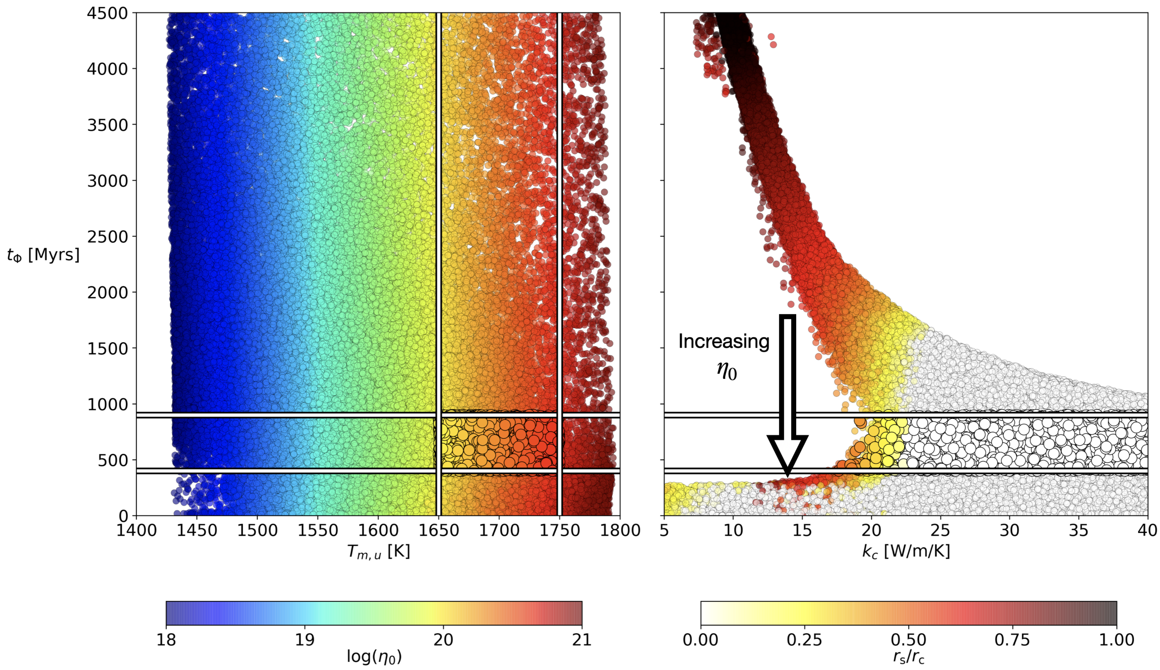

Figure 2. Monte-Carlo simulation results. Left panel shows cessation time, t_Φ, plotted against present day upper mantle temperature, $T_{\mathrm{m,u}}$. White lines indicate the limits from observational constraints and the colour scale indicates the value of $\log(\eta_0)$. On both panels, successful models are indicated by the larger opaque circles. Right panel shows t_Φ against core conductivity, with the same limits on t_Φ as the left panel. Models where the dynamo is active at present have no cessation time and so do not appear on the figure. Colour scale indicates the proportion of the core that is convecting at present, given by the ratio of radii of the base of the stable layer, r_{s}, and the CMB, r_{c} (0 = fully conductive core, 1 = fully convecting core). Downwards arrow indicates how t_Φ varies with η_0 if all other input parameters are fixed.

The right panel of Figure 2 shows how all 2010 successful models are limited to the upper half of core conductivities we have considered. At $k_{\mathrm{c}} < 20$ W m^{-1}K^{-1}, there are two branches between models that have dynamo that fails too early or lives too long. The upper branch can be explained by the long term decaying trend in Q_{c} and the approximately constant value of Q_{a}, as can be seen in the reference example case in Figure 1a. Since t_Φ occurs when $Q_{\mathrm{c}} \sim Q_{\mathrm{a}}$, as k_{c} (and hence Q_{a}) is decreased, dynamo failure is delayed. At the lower branch where the dynamo is short lived, models have the highest viscosities (high η_0 and low $T_{\mathrm{m,0}}$) and/or low initial superheats ΔT. These conditions lead to low CMB heat flows that quickly become sub-isentropic and hence an early t_Φ. The absence of models inbetween the branches arises from the behaviour of Q_{c} at higher mantle viscosities, as seen in the high viscosity case in Figure 1a. At low k_{c}, a sufficiently large viscosity is needed to produce $Q_{\mathrm{c}} < Q_{\mathrm{a}}$. However, this results in the mantle heating up early in the evolution since heat cannot be efficiently moved out the top of the mantle to counter the radiogenic heating. This heating in turn reduces the viscosity, allowing Q_{c} to increase over time before falling again at a later time (see high viscosity case in Fig.1a). The inflexion in Q_{c} ensures that t_Φ is either very late on, or very early after the initial drop in Q_{c} since this plateau lasts for ~ 1 Gyr. For $k_{\mathrm{c}} > 20$ W m^{-1}K^{-1}, Q_{a} is sufficiently large that lower viscosities not exhibiting this inflexion in Q_{c} are sufficient to provide the desired range of t_Φ.

The colour-scale on the right panel of Figure 2 indicates the proportion of the core that is convecting at present day. We find all successful models with $k_c > 24$ W m^{-1}K^{-1} are fully stratified, with successful models with a lower k_c having a stable layer comprising at least the top half of the core. Typically models that are fully stratified at present, have been fully stratified for 100's Myr, cooling purely by conduction. In all of our models the core is far hotter than the melting point observed by Gilfoy and Li (2020), with the successful models giving $T_c = 1940-2080$ K. Our temperatures are also above the melting point given by Stewart et al. (2007) and those used by Rivoldini et al. (2011); Hemingway and Driscoll (2021) for sulphur concentrations consistent with interior models, > 10 wt% (Rivoldini et al., 2011; Khan et al., 2018).

For the mantle thermal conductivity, we have used the recent experiments on iron rich olivine predicted for the Martian mantle (Zhang et al., 2019) (Table S1) although this differs from the typical value of 4 W m^{-1}K^{-1} used in thermal evolution models (e.g. Williams & Nimmo, 2004; Breuer & Spohn, 2003; Thiriet et al., 2019). We ran our Monte-Carlo simulations with the mantle thermal conductivity set to 4 W m^{-1}K^{-1} to investigate the impact. The same behaviour was observed with regards to where successful models are located in the parameter space. The successful model with the lowest k_c was 12.5 W m^{-1}K^{-1}, as opposed to 17.5 W m^{-1}K^{-1} seen in Figure 2b. Since the study of Zhang et al. (2019) account for the higher iron content of Martian mantle as well as the extended olivine phase due to lower gravity than Earth, we focus on the results that are based on their estimates.

Figure 3 demonstrates the general impact of varying any one of the four variables in Table 1 upon t_Φ and $T_{m,u}$ relative to the reference case in Figure 1. The present day temperature of the mantle is almost exclusively controlled by η_0 which also exerts some control on the dynamo cessation time. The other inputs, $T_{m,u}$, k_c, and ΔT, instead almost solely influence the cessation time, with the largest influence on t_Φ coming from k_c.

Finally, successful models all predict a heat flow conducted through the stagnant lid of around 15 mW m^2, although this is a consequence of the thermal evolution being insensitive to the size of the stagnant lid and a constrained temperature at the base of the lid. If we had imposed a different stagnant lid size, the predicted heat flow would change accordingly, as we have assumed a linear temperature gradient across it.

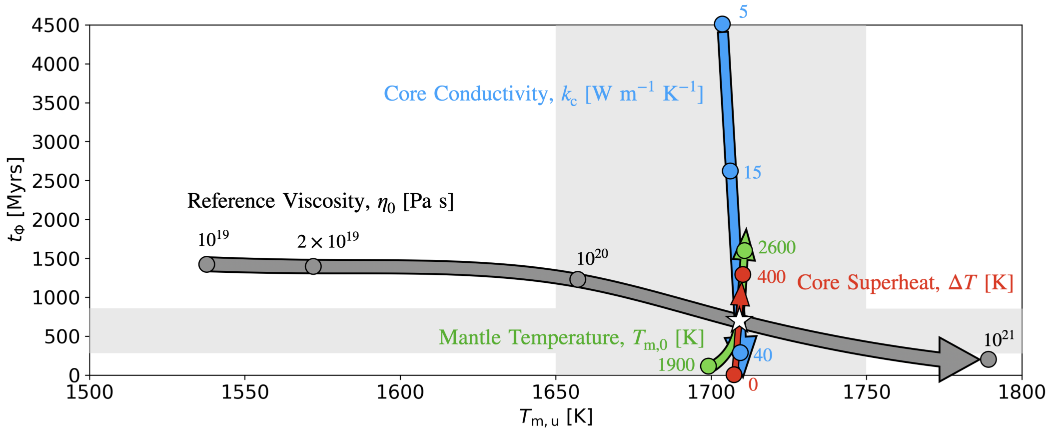

Figure 3. Influence of the 4 varied inputs ($T_{\mathrm{m,0}}$, ΔT, k_{c}, η_0) t_Φ and $T_{\mathrm{m,u}}$. Shaded regions indicate constraints upon t_Φ and $T_{\mathrm{m,u}}$. The star marks the reference case shown in Figure 1. Arrows and circular data points show the influence of the variable (indicated by colour) if only that variable is changed from the reference case. For example, the bottom right point marked 10^{21}, shows the results using all inputs the same as the reference case, except that η_0 is changed to 10^{21} Pa s.

4 Discussion and Conclusions

Our results suggest that a value of $k_{\mathrm{c}} \geq 18$ W m^{-1} K^{-1} is required for the dynamo to stop between 400 and 900 Myrs after core formation. Studies of pure iron have suggested k_{c} upwards of 80 W m^{-1} K^{-1} (Deng et al., 2013; Pommier, 2018; Ezenwa & Yoshino, 2021), with alloying light elements reducing k_{c} (Pommier, 2020) and so our lower limit of 18 W m^{-1} K^{-1} can be related to the light elements in the core. Using electrical measurements, Pommier (2018) obtained a value of $k_{\mathrm{c}} \approx 40$ W m^{-1} K^{-1} for Fe with 5 wt% S (Fe-5S). Due to the large amount of FeO in the Martian mantle (Wänke & Dreibus, 1994), significant amounts of oxygen may have dissolved into the core (Tsuno et al., 2007) and an additional 0.5 wt% oxygen to Fe-5S drastically reduces k_{c} to ≈ 18 W m^{-1} K^{-1} at 2000 K (Pommier et al., 2020). Furthermore, nickel in the core, whilst weakly impacting many properties of iron such as density, can significantly reduce k_{c} as well as the melting temperature (Gilfoy & Li, 2020). Pommier (2020) observed 10 wt% Ni alloyed with Fe-5S also halves k_{c} to ≈ 20 W m^{-1} K^{-1} compared to just Fe-5S. Although the experiments discussed in this section were conducted at 8-10 GPa, lower than the 20-40 GPa in the Martian core, k_{c} reduces by approximately 10% when extrapolated to 20-40 GPa (Pommier et al., 2020). Since > 15 wt% of sulphur is predicted based on density estimates in the Martian core (Rivoldini et al., 2011; Khan et al., 2018), a lower k_{c} than 18 W m^{-1} K^{-1} may be expected, highlighting the need to further explore k_{c} as a function of composition and pressure to interpret the magnetic history of Mars.

Inference of the dynamo cessation time from our evolution models is dependent upon the scenario for cooling of the planet, where we have assumed stagnant lid convection in the mantle. Early plate tectonics has been proposed based upon observations of geological structures in the northern lowlands (Sleep, 1994) and magnetic anomalies in the southern highlands (Connerney et al., 1999) that were hypothesised to indicate ancient sea floor spreading. Plate tectonics would allow the mantle to cool more rapidly, increasing the heat flow from the core (Nimmo & Stevenson, 2000). Little evidence of plate tectonics has been subsequently discovered and any significant period of plate tectonics appears incompatible with the present day crustal thickness (Breuer & Spohn, 2003). Given available information, assuming the stagnant lid regime for all time seems reasonable.

An alternative scenario proposes that a series of large impacts on Mars heated the mantle (Roberts et al., 2009) and thermally stratified the top of the core (Arkani-Hamed & Olson, 2010; Roberts & Arkani-Hamed, 2014) which could have triggered an already sub-critical dynamo to quickly fail (Kuang et al., 2008). The core may take 10's Myr to 1 Gyr (Arkani-Hamed & Olson, 2010; Roberts & Arkani-Hamed, 2014) for convection to re-establish in the entire core, hence Q_c may be super-isentropic for up to 1 Gyr whilst still being compatible with the inferred cessation time for Mars. Taking the most generous estimate that impacts could have inhibited a super-isentropic heat flow from producing a dynamo for 1 Gyr would change our interpretation by essentially shifting the results in Figure 2 down on the y-axis by 1 Gyr. Due to the rapid increase in t_Φ with decreasing k_c, the right panel of Figure 2 would instead give a lower bound on successful models of ~ 15 W m^{-1} K^{-1}, rather than 18 W m^{-1} K^{-1}. We therefore expect giant impacts to not significantly alter our results, assuming the evolution of the mantle on the Gyr timescale is also not significantly altered.

In writing equation 2 we have included only a temperature dependence on the viscosity. Water content of olivine crystals can significantly impact η (Mackwell et al., 1985), particularly in the Fe rich Martian mantle (Kohlstedt & Mackwell, 2010), which to some extent is captured by our consideration of a wide range for η_0. What we fail to account for is any time dependence on the viscosity except through the temperature, yet in the absence of sufficient evidence of changing water content in the mantle we cannot include this effect at this stage.

All of our successful models contain a thermally stratified layer at least comprising the top half of the core, with the majority producing a fully conductive core. Inversions for the Martian interior typically assume the core is isentropic (e.g. Khan et al., 2018) but we suggest this constraint should be relaxed by studies in the future. Our estimates on the CMB temperature based on successful models (2010 ± 70 K) may also help in this regard.

In summary, we have conducted a suite of models for the thermal evolution of Mars including thermal stratification in the core and considering a range of core thermal conductivities based on recent experimental data. We demonstrated that in order to match estimates of the termination of the Martian dynamo, the thermal conductivity is limited to $k_c < 18$ W m^{-1}K^{-1}. This limit will aid future constraints upon the composition of the core since light elements core strongly influence k_c. We find at least the upper 50% of the core to be thermally stratified, with the majority of models predicting the entire core to be conductive with a CMB temperature of 2010 ± 70 K. Finally, we utilised recent temperature constraints of the present day mantle as an additional constraint which limits the range of successful solutions since it constrained the viscosity of the mantle to $\eta_0 = 10^{20} - 10^{21}$ Pa s in our modelling framework.

References

Acuna, M., Connerney, J., Wasilewski, P. a., Lin, R., Anderson, K., Carlson, C., ... others (1998). Magnetic field and plasma observations at mars: Initial results of the mars global surveyor mission. *Science*, *279*(5357), 1676–1680.

Arkani-Hamed, J., & Olson, P. (2010). Giant impact stratification of the martian core. *Geophysical research letters*, *37*(2).

Breuer, D., & Spohn, T. (2003). Early plate tectonics versus single-plate tectonics on mars: Evidence from magnetic field history and crust evolution. *Journal of Geophysical Research: Planets*, *108*(E7).

Breuer, D., & Spohn, T. (2006). Viscosity of the martian mantle and its initial temperature: Constraints from crust formation history and the evolution of the magnetic field. *Planetary and Space Science*, *54*(2), 153–169.

Connerney, J., Acuna, M., Wasilewski, P. J., Ness, N. F., Reme, H., Mazelle, C., ...

Cloutier, P. (1999). Magnetic lineations in the ancient crust of mars. *Science*, *284*(5415), 794–798.
Davies, C. J., & Pommier, A. (2018). Iron snow in the martian core? *Earth and Planetary Science Letters*, *481*, 189–200.
Deng, L., Seagle, C., Fei, Y., & Shahar, A. (2013). High pressure and temperature electrical resistivity of iron and implications for planetary cores. *Geophysical Research Letters*, *40*(1), 33–37.
Ezenwa, I. C., & Yoshino, T. (2021). Martian core heat flux: Electrical resistivity and thermal conductivity of liquid fe at martian core pt conditions. *Icarus*, *360*.
Fraeman, A. A., & Korenaga, J. (2010). The influence of mantle melting on the evolution of mars. *Icarus*, *210*(1), 43–57.
Gilfoy, F., & Li, J. (2020). Thermal state and solidification regime of the martian core: Insights from the melting behavior of feni-s at 20 gpa. *Earth and Planetary Science Letters*, *541*, 116285.
Greenwood, S., Davies, C., & Mound, J. (2021). On the evolution of thermally stratified layers at the top of Earth's core.
(Preprint available on arXiv)
Gubbins, D., Alfe, D., Masters, G., Price, G., & Gillan, M. (2003). Can the Earth's dynamo run on heat alone? , *155*, 609–622.
Hemingway, D. J., & Driscoll, P. E. (2021). History and future of the martian dynamo and implications of a hypothetical solid inner core. *Journal of Geophysical Research: Planets*, *126*(4), e2020JE006663.
Karato, S.-i., & Wu, P. (1993). Rheology of the upper mantle: A synthesis. *Science*, *260*(5109), 771–778.
Khan, A., Liebske, C., Rozel, A., Rivoldini, A., Nimmo, F., Connolly, J., ... Giardini, D. (2018). A geophysical perspective on the bulk composition of mars. *Journal of Geophysical Research: Planets*, *123*(2), 575–611.
Kohlstedt, D., & Mackwell, S. (2010). Strength and deformation of planetary lithospheres. *Planetary tectonics*, 397–456.
Kuang, W., Jiang, W., & Wang, T. (2008). Sudden termination of martian dynamo?: Implications from subcritical dynamo simulations. *Geophysical Research Letters*, *35*(14).
Labrosse, S., Poirier, J.-P., & Le Mouël, J.-L. (1997). On cooling of the Earth's core. *Physics of the Earth and Planetary Interiors*, *99*, 1–17.
Langlais, B., Thébault, E., Houliez, A., Purucker, M. E., & Lillis, R. J. (2019). A new model of the crustal magnetic field of mars using mgs and maven. *Journal of Geophysical Research: Planets*, *124*(6), 1542–1569.
Langlais, B., Thebault, E., Ostanciaux, E., & Mangold, N. (2012). A late martian dynamo cessation time 3.77 gy ago. In *Lunar and planetary science conference* (p. 1231).
Mackwell, S., Kohlstedt, D., & Paterson, M. (1985). The role of water in the deformation of olivine single crystals. *Journal of Geophysical Research: Solid Earth*, *90*(B13), 11319–11333.
Milbury, C., Schubert, G., Raymond, C., Smrekar, S., & Langlais, B. (2012). The history of mars' dynamo as revealed by modeling magnetic anomalies near tyrrhenus mons and syrtis major. *Journal of Geophysical Research: Planets*, *117*(E10).
Mittelholz, A., Johnson, C., Feinberg, J., Langlais, B., & Phillips, R. (2020). Timing of the martian dynamo: New constraints for a core field 4.5 and 3.7 ga ago. *Science Advances*, *6*(18), eaba0513.
Nimmo, F. (2015). Thermal and compositional evolution of the core. In G. Schubert (Ed.), *Treatise on Geophysics 2nd edn, vol. 9* (pp. 209–219). Elsevier, Amsterdam.

Nimmo, F., & Stevenson, D. (2000). Influence of early plate tectonics on the thermal evolution and magnetic field of mars. *Journal of Geophysical Research: Planets*, *105*(E5), 11969–11979.
Plesa, A.-C., Padovan, S., Tosi, N., Breuer, D., Grott, M., Wieczorek, M., ... Banerdt, W. (2018). The thermal state and interior structure of mars. *Geophysical Research Letters*, *45*(22), 12–198.
Plesa, A.-C., Tosi, N., Grott, M., & Breuer, D. (2015). Thermal evolution and urey ratio of mars. *Journal of Geophysical Research: Planets*, *120*(5), 995–1010.
Pommier, A. (2018). Influence of sulfur on the electrical resistivity of a crystallizing core in small terrestrial bodies. *Earth and Planetary Science Letters*, *496*, 37–46.
Pommier, A. (2020, 07). Experimental investigation of the effect of nickel on the electrical resistivity of Fe-Ni and Fe-Ni-S alloys under pressure. *American Mineralogist*, *105*(7), 1069-1077. Retrieved from `https://doi.org/10.2138/am-2020-7301` doi: 10.2138/am-2020-7301
Pommier, A., Davies, C. J., & Zhang, R. (2020). A joint experimental-modeling investigation of the effect of light elements on dynamos in small planets and moons. *Journal of Geophysical Research: Planets*, *125*(8).
Rivoldini, A., Van Hoolst, T., Verhoeven, O., Mocquet, A., & Dehant, V. (2011). Geodesy constraints on the interior structure and composition of mars. *Icarus*, *213*(2), 451–472.
Roberts, J. H., & Arkani-Hamed, J. (2014). Impact heating and coupled core cooling and mantle dynamics on mars. *Journal of Geophysical Research: Planets*, *119*(4), 729–744.
Roberts, J. H., Lillis, R. J., & Manga, M. (2009). Giant impacts on early mars and the cessation of the martian dynamo. *Journal of Geophysical Research: Planets*, *114*(E4).
Sleep, N. H. (1994). Martian plate tectonics. *Journal of Geophysical Research: Planets*, *99*(E3), 5639–5655.
Stevenson, D. J. (2001). Mars' core and magnetism. *Nature*, *412*(6843), 214–219.
Stewart, A. J., Schmidt, M. W., Van Westrenen, W., & Liebske, C. (2007). Mars: A new core-crystallization regime. *Science*, *316*(5829), 1323–1325.
Thiriet, M., Breuer, D., Michaut, C., & Plesa, A.-C. (2019). Scaling laws of convection for cooling planets in a stagnant lid regime. *Physics of the Earth and Planetary Interiors*, *286*, 138–153.
Tsuno, K., Ohtani, E., & Terasaki, H. (2007). Immiscible two-liquid regions in the fe–o–s system at high pressure: implications for planetary cores. *Physics of the Earth and Planetary Interiors*, *160*(1), 75–85.
Wänke, H., & Dreibus, G. (1994). Chemistry and accretion history of mars. *Philosophical Transactions of the Royal Society of London. Series A: Physical and Engineering Sciences*, *349*(1690), 285–293.
Williams, J.-P., & Nimmo, F. (2004). Thermal evolution of the martian core: Implications for an early dynamo. *Geology*, *32*(2), 97–100.
Zhang, Y., Yoshino, T., Yoneda, A., & Osako, M. (2019). Effect of iron content on thermal conductivity of olivine with implications for cooling history of rocky planets. *Earth and Planetary Science Letters*, *519*, 109–119.

Acknowledgments

SG, CD and AP recognise support from the joint NSF-NERC grant 1832462 (NERC reference NE/T003855/1). We thank Josef Gutierrez for useful discussions of the material properties of the Martian mantle. Data from the Monte-Carlo simulations in this paper are available at https://doi.org/10.5281/zenodo.5109504

Supporting Information for "Influence of thermal stratification on the structure and evolution of the Martian core."

Sam Greenwood[1], Christopher J. Davies[1], Anne Pommier[2,3]

[1]School of Earth and Environment, University of Leeds, Leeds, UK

[2]Scripps Institution of Oceanography, University of California San Diego, La Jolla, CA, USA

[3]Earth and Planets Laboratory, Carnegie Institution for Science, Washington, DC, USA

Contents of this file

Text S1.

The entropy budget is used to estimate the ohmic dissipation, E_{J}, produced by magnetic field generation (Gubbins et al., 2003; Williams & Nimmo, 2004; Greenwood et al., 2021):

$$\overbrace{\int k_{\mathrm{c}} \left(\frac{\nabla T}{T}\right)^2 \mathrm{d}V_{\mathrm{c}}}^{E_{\mathrm{k}}} + \overbrace{\int \frac{\Phi}{T} \mathrm{d}V_{\mathrm{c}}}^{E_{\mathrm{J}}} = \overbrace{-\int \left(\frac{1}{T_{\mathrm{c}}} - \frac{1}{T}\right) \rho_c C_{p,c} \frac{\partial T}{\partial t} \mathrm{d}V_{\mathrm{c}},}^{E_{\mathrm{s}}} \quad (1)$$

Corresponding author: S. Greenwood (s.greenwood@leeds.ac.uk

where T is temperature and T_{c} is the temperature at the CMB. Terms are integrated over the volume of the entire core, V_{c}, with the temperature and cooling rate defined by a conduction solution in the stable layer ($r_{\mathrm{s}} \leq r \leq r_{\mathrm{c}}$) or by the isentropic value in the convecting region ($0 \leq r \leq r_{\mathrm{s}}$). Φ is the heat released by ohmic dissipation.

The entropy gain in the core from ohmic dissipation must be > 0; the process is a dissipative one and so can only act to increase entropy. Assuming the entire core is convecting at all times can lead to an inconsistency producing negative values for E_{J} (Pozzo et al., 2012). We note that when including a thermally stable layer with a conduction profile rather than an isentropic profile when $Q_{\mathrm{c}} < Q_{\mathrm{a}}$, ensures $E_{\mathrm{J}} \geq 0$ as is physically expected (as seen in the main document).

Typically, the condition $E_{\mathrm{J}} > 0$ is used to infer dynamo action (Williams & Nimmo, 2004, e.g.) but we cannot use this since we do not obtain $E_{\mathrm{J}} \leq 0$. Physically, dynamo action would not necessarily be expected at some small value of E_{J} since a dynamo requires sufficiently established, self-sustaining feedback between the magnetohydrodynamic processes. Such an established process would produce a certain minimum of ohmic dissipation that for the Earth has been estimated to be on the order of 1 MW K^{-1} (Jackson et al., 2011). Therefore, we take $E_{\mathrm{J}} > 1$ MW K^{-1} as our requirement for an active dynamo. The precise value of this lower bound does not significantly change t_{Φ} since the variations of E_{J} brought about by the secular cooling of the core are generally much larger than this value.

References

Gilfoy, F., & Li, J. (2020). Thermal state and solidification regime of the martian core:

Insights from the melting behavior of feni-s at 20 gpa. *Earth and Planetary Science Letters*, *541*, 116285.

Greenwood, S., Davies, C., & Mound, J. (2021). On the evolution of thermally stratified layers at the top of Earth's core.

(Preprint available on arXiv)

Gubbins, D., Alfe, D., Masters, G., Price, G., & Gillan, M. (2003). Can the Earth's dynamo run on heat alone? , *155*, 609–622.

Jackson, A., Livermore, P. W., & Ierley, G. (2011). On ohmic heating in the earth's core ii: Poloidal magnetic fields obeying taylor's constraint. *Physics of the Earth and Planetary Interiors*, *187*(3-4), 322–327.

Khan, A., Liebske, C., Rozel, A., Rivoldini, A., Nimmo, F., Connolly, J., ... Giardini, D. (2018). A geophysical perspective on the bulk composition of mars. *Journal of Geophysical Research: Planets*, *123*(2), 575–611.

Pozzo, M., Davies, C., Gubbins, D., & Alfe, D. (2012). Thermal and electrical conductivity of iron at earth's core conditions. *Nature*, *485*(7398), 355–358.

Thiriet, M., Breuer, D., Michaut, C., & Plesa, A.-C. (2019). Scaling laws of convection for cooling planets in a stagnant lid regime. *Physics of the Earth and Planetary Interiors*, *286*, 138–153.

Williams, J.-P., & Nimmo, F. (2004). Thermal evolution of the martian core: Implications for an early dynamo. *Geology*, *32*(2), 97–100.

Zhang, Y., Yoshino, T., Yoneda, A., & Osako, M. (2019). Effect of iron content on thermal conductivity of olivine with implications for cooling history of rocky planets.

Earth and Planetary Science Letters, *519*, 109–119.

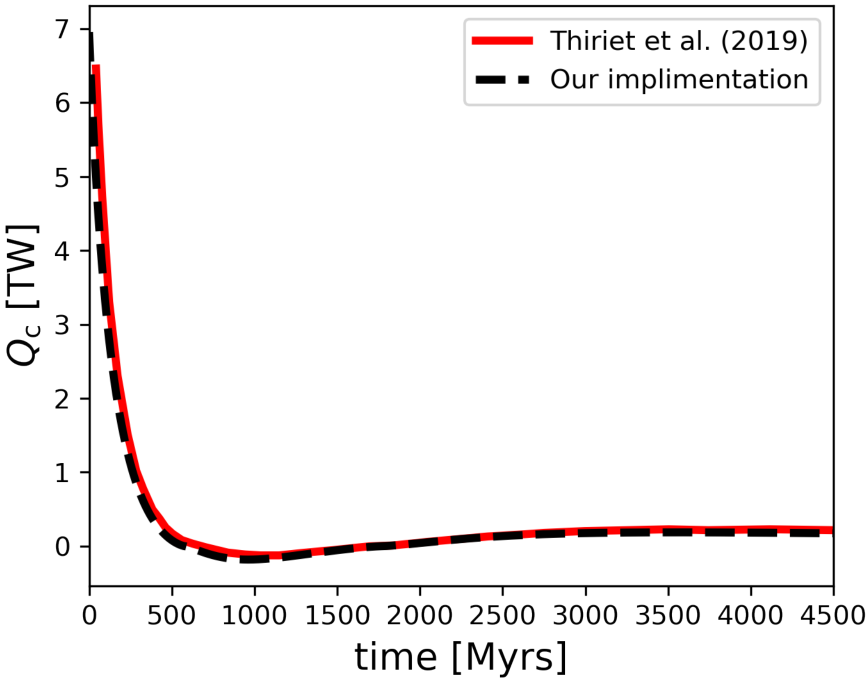

Figure S1. Recreation of results from Figure 2 of Thiriet et al. (2019) showing the CMB heat flow through time. All parameters are the same, as well as using the same core model (simple secular cooling of an isothermal core), as Thiriet et al. (2019), with the only difference being that we assumed a fixed stagnant lid of 300 km, rather than implementing their time dependent calculation. Our solution does not appreciably change when using a lid thickness between 200-400 km.

Table S1. Table S1 lists all fixed parameters using for all models produced in our Monte-Carlo simulation.

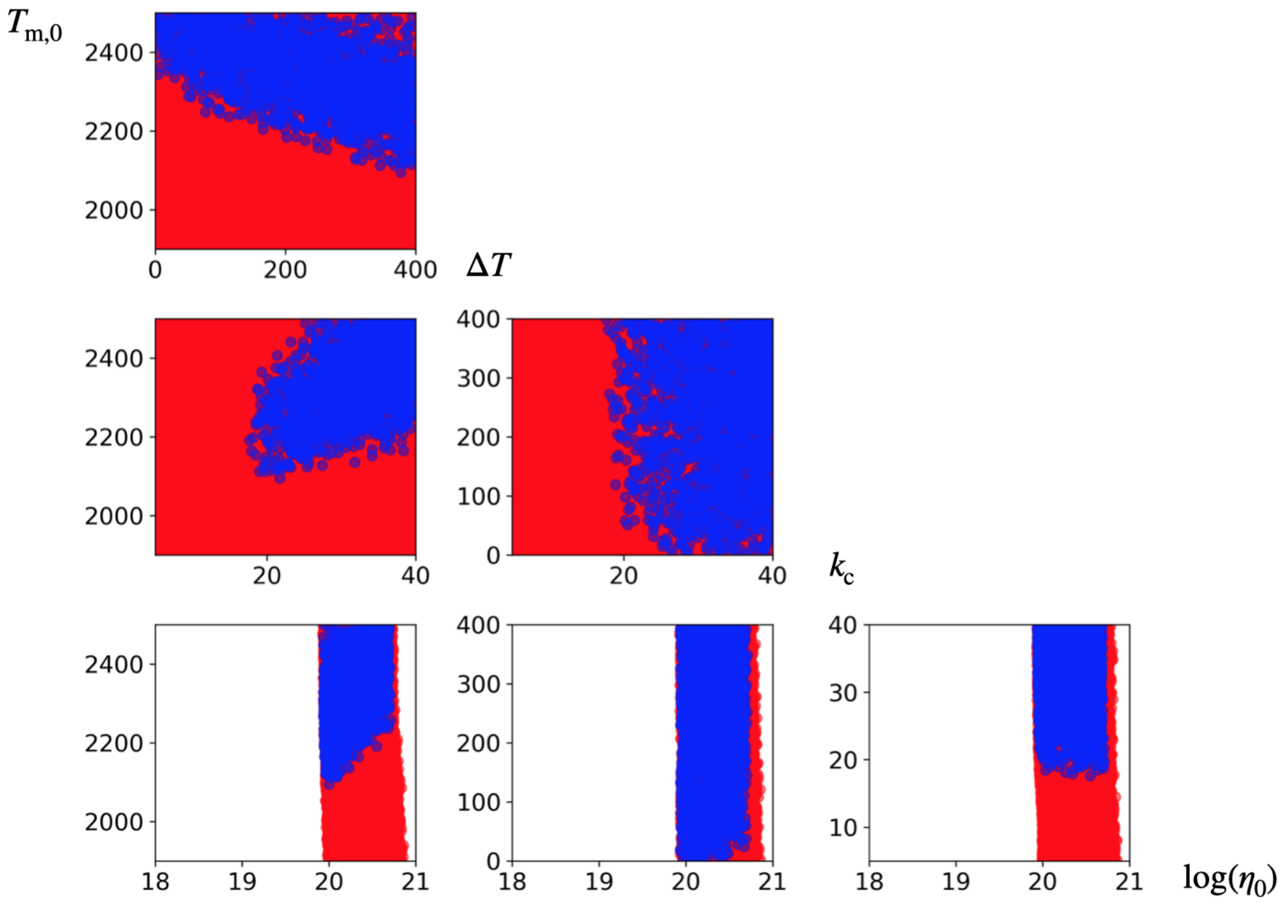

Figure S2. Models fitting our temperature constraint (red) and models that fit both the temperature and magnetic history constraints (red) with combinations of the 4 variables: $T_{\mathrm{m},0}$, ΔT, k_{c}, and η_0. Axis labels indicate the variable on the axis in that row/column.

Table S1. Fixed input parameters for all model runs.

Parameter	Symbol	Value	Units	Reference
Core radius	r_c	1750	km	Khan et al. (2018)
Core density	ρ_c	6100	$\mathrm{kgm^{-3}}$	Khan et al. (2018)
Core thermal expansivity	$\alpha_{T,c}$	10^{-5}	$\mathrm{K^{-1}}$	-
Core heat capacity	$C_{p,c}$	1089	$\mathrm{Jkg^{-1}K^{-1}}$	Gilfoy and Li (2020)
Radius of Mars	r_m	3400	km	-
Stagnant lid thickness	D_{sl}	300	km	Khan et al. (2018)
Mantle density	ρ_m	3550	$\mathrm{kgm^{-3}}$	Khan et al. (2018)
Upper mantle thermal conductivity	$k_{m,u}$	2	$\mathrm{W\ m^{-1}K^{-1}}$	Zhang, Yoshino, Yoneda, and Osako (2019)
Lower mantle thermal conductivity	$k_{m,l}$	5	$\mathrm{W\ m^{-1}K^{-1}}$	Zhang et al. (2019)
Mantle thermal expansivity	$\alpha_{T,m}$	2.65×10^{-5}	$\mathrm{K^{-1}}$	Zhang et al. (2019)
Mantle heat capacity	$C_{p,m}$	798	$\mathrm{Jkg^{-1}K^{-1}}$	Zhang et al. (2019)
Activation energy	A	300	$\mathrm{kJmol^{-1}}$	-
Convection scaling parameters	a, β	2.54, 0.335	-	Thiriet et al. (2019)